

Novel method for the direct measurement of the τ lepton dipole moments

J. Fu,¹ M.A. Giorgi,² L. Henry,³ D. Marangotto,¹ F. Martínez Vidal,³ A. Merli,¹ N. Neri,¹ and J. Ruiz Vidal³

¹*INFN Sezione di Milano and Università di Milano, Milano, Italy*

²*INFN Sezione di Pisa and Università di Pisa, Pisa, Italy*

³*IFIC, Universitat de València-CSIC, Valencia, Spain*

(Dated: December 15, 2024)

A novel method for the direct measurement of the elusive magnetic and electric dipole moments of the τ lepton is presented. The experimental approach relies on the production of τ^+ leptons from $D_s^+ \rightarrow \tau^+ \nu_\tau$ decays, originated in fixed-target collisions at the LHC. A sample of polarized τ^+ leptons is kinematically selected and subsequently channeled in a bent crystal. The magnetic and electric dipole moments of the τ^+ lepton are measured by determining the rotation of the spin-polarization vector induced by the intense electromagnetic field between crystal atomic planes. The experimental layout and analysis technique are discussed, along with the expected sensitivities.

PACS numbers: 13.35.Dx, 13.40.Em, 14.60.Fg

The magnetic (MDM) and electric (EDM) dipole moments are among the most prominent static properties of elementary particles. Their measurements for common particles like the electron, muon and nucleons, combined with precise theoretical calculations, have provided stringent tests of physics within and beyond the Standard Model (SM) [1–8]. For the τ lepton the territory is uncharted due to the difficulties imposed by its short lifetime ($\approx 3 \times 10^{-13}$ s) that prevents the use of spin-precession technique adopted in the muon $g - 2$ experiment [3, 4]. In the recent years considerable attention has received the possibility of measuring directly the electromagnetic dipole moments of short-lived baryons originated in fixed-target collisions at the LHC and subsequently channeled in bent crystals [9–14]. Firstly suggested in Ref. [15] using $B^+ \rightarrow \tau^+ \nu_\tau$ decays, in this Letter we assess that this method can be applied to τ^+ leptons produced in $D_s^+ \rightarrow \tau^+ \nu_\tau$ decays with much greater yield. The MDM (EDM) is defined as $\boldsymbol{\mu} = g\mu_\tau \mathbf{s}/2$ ($\boldsymbol{\delta} = d\mu_\tau \mathbf{s}/2$), where $\mu_\tau = e\hbar/(2m_\tau c)$ is the lepton magneton, g (d) is the gyromagnetic (gyroelectric) factor, and \mathbf{s} is the spin-polarization vector [16]. In the SM, the τ anomalous MDM is expected to be $a = (g-2)/2 \approx 10^{-3}$, and its EDM, d , to be minuscule. However, the dipole moments can be largely enhanced in presence of physics beyond the SM [17–19]. Indirect methods based on precise measurements of $\tau^+ \tau^-$ pair production cross sections in $e^+ e^-$ annihilation achieved an accuracy on a of few percent level [20, 21], more than one order of magnitude above the SM prediction [18], and lead limits on d at 10^{-16} e cm level [20, 22].

In this Letter, we propose a novel method for the direct measurement of both the MDM and EDM of the τ^+ lepton, and a technique to extract its polarization. The proposed solution features a large production cross-section of high-energy (≈ 1 TeV) τ^+ leptons produced in

$D_s^+ \rightarrow \tau^+ \nu_\tau$ decays, originated in proton fixed-target collisions at the LHC. The τ^+ leptons are reconstructed in $\tau^+ \rightarrow \pi^+ \pi^- \pi^+ \bar{\nu}_\tau$ (indicated as $3\pi \bar{\nu}_\tau$ in the following) decays. A bent crystal is employed to exploit the channeling phenomenon of positively-charged particles aligned with the crystal atomic planes within few μrad [23]. The intense electric field between the atomic planes of the bent crystal induces spin precession for the short-lived τ^+ lepton. The angular momentum conservation in the D_s^+ weak decay imposes negative helicity for the τ^+ lepton in the D_s^+ rest frame. The selection of τ^+ leptons emitted with positive θ angles with respect to the D_s^+ mesons flight direction z (see Fig. 1), produces an enhancement of the degree of polarization along the perpendicular y axis. A negative polarization, $s_z \approx \beta/\beta^* \approx -10\%$, along the z axis is induced by the Lorentz boost that makes the acceptance larger for the forward- than for the backward-emitted τ^+ . Here, β (β^*) is the velocity of the D_s^+ (τ^+) in the laboratory (D_s^+ rest) frame. The selection of the highest momentum candidates produces the enhancement of the s_z polarization thanks to the increase of the population of forward emitted τ^+ . The interaction of the MDM (EDM) with the crystal electric field induces the spin rotation in the bending plane (plane perpendicular to the bending plane). A novel analysis technique based on a multivariate classifier using reconstructed kinematic variables of the τ^+ decay products is employed to determine the rotation of the spin-polarization vector.

The main advantage of producing τ^+ leptons in fixed-target collisions at the LHC consists in a large Lorentz boost, crucial for a measurable spin precession of short-lived particles channeled in a bent crystal. The vast majority of τ^+ leptons produced in p -W interactions at $\sqrt{s} \approx 115$ GeV arises from $D_s^+ \rightarrow \tau^+ \nu_\tau$ decays, and the corresponding cross section is estimated to be $\sigma[pp \rightarrow D_s^+(\rightarrow \tau^+ \nu_\tau)X] \approx 1.96 \mu\text{b}$. The following in-

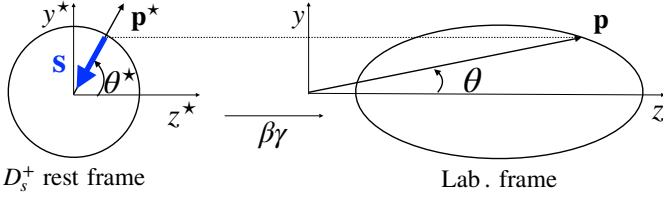


FIG. 1: Negative helicity τ^+ leptons produced in the $D_s^+ \rightarrow \tau^+ \nu_\tau$ decay, emitted at angle θ^* in the D_s^+ rest frame and corresponding angle θ in the laboratory frame, with $\tan \theta = \tan \theta^* / \{\gamma[1 + \beta/(\beta^* \cos \theta^*)]\}$ and $\beta\gamma \gg 1$ the Lorentz boost factor.

puts are used: the total charm production cross section measured by LHCb at $\sqrt{s} = 86.6$ GeV [24] in p -He collisions, $\sigma_{c\bar{c}} = (287.8 \pm 8.5 \pm 25.7)$ $\mu\text{b/nucleon}$, and rescaled to $\sqrt{s} = 114.6$ GeV assuming a linear dependence on \sqrt{s} ; the fragmentation fraction $f(c \rightarrow D_s^+) = (9.25 \pm 0.82)\%$ [25, 26]; and the branching fraction $\mathcal{B}(D_s^+ \rightarrow \tau^+ \nu_\tau) = (5.55 \pm 0.24)\%$ [27].

The rate of τ^+ produced by 7 TeV protons on a 1 cm thick tungsten (W) fixed target is estimated

$$\frac{dN_{\tau^+}}{dt} = \frac{F}{S} \sigma [pp \rightarrow D_s^+ (\rightarrow \tau^+ \nu_\tau) X] N_T, \quad (1)$$

where F is the proton rate, S the beam transverse area, and $N_T = N_A \rho S A_N / A_T$ the number of target nucleons. For the latter, N_A is the Avogadro number, ρ the target density, and A_T (A_N) the atomic mass (mass number). A beam of protons with rate $F = 10^9$ Hz impinging on the target would produce ≈ 22.700 τ^+ /s, with ≈ 2.100 τ^+ /s decaying into the $3\pi \bar{\nu}_\tau$ final state, considering the branching fraction $\mathcal{B}(\tau^+ \rightarrow 3\pi \bar{\nu}_\tau) = (9.31 \pm 0.05)\%$ [27]. This yields a proton to $\tau^+ \rightarrow 3\pi \bar{\nu}_\tau$ conversion factor of 2.1×10^{-6} .

The τ^+ spin-polarization vector \mathbf{s} in any reference frame can be determined from the squared decay amplitude of the $D_s^+ \rightarrow \tau^+ \nu_\tau$ decay [16, 28, 29]. In a reference frame attached to the crystal and comoving with the channeled particle, where the spin precession takes place, it is given by the unit vector along the D_s^+ momentum in the τ^+ rest frame. Expressed in laboratory quantities,

$$\mathbf{s} = \frac{1}{\omega} \left(m_\tau \mathbf{q} - q_0 \mathbf{p} + \frac{\mathbf{q} \cdot \mathbf{p}}{p_0 + m_\tau} \mathbf{p} \right), \quad (2)$$

where \mathbf{p} (\mathbf{q}) is the momentum of the τ^+ (D_s^+), p_0 (q_0) its energy, and $\omega = (m_{D_s}^2 - m_\tau^2)/2$, with m_{D_s} the D_s mass. In the following, we assume that the crystal orientation is defined by axes $(\mathbf{x}, \mathbf{y}, \mathbf{z})$, the bending taking place in the \mathbf{yz} plane, the crystal \mathbf{y} (\mathbf{z}) axis tilted by an angle θ_y with respect to the laboratory y (z) axis, and the protons impinging along the z axis, *i.e.* $\mathbf{z} = (0, \sin \theta_y, \cos \theta_y)$, $\mathbf{y} = (0, \cos \theta_y, -\sin \theta_y)$, $\mathbf{x} = (1, 0, 0)$. The projections of

\mathbf{s} are then given by

$$\begin{aligned} s_{0,x} &\approx \frac{m_\tau |\mathbf{q}|}{\omega} \theta_{x,D_s\tau}, \\ s_{0,y} &\approx \frac{m_\tau |\mathbf{q}|}{\omega} \sin \theta_{y,D_s\tau}, \\ s_{0,z} &\approx s_{0,\parallel} = \frac{1}{\omega} (-q_0 |\mathbf{p}| + |\mathbf{q}| p_0 \cos \theta_{D_s\tau}), \end{aligned} \quad (3)$$

where $s_{0,\parallel}$ refers to the projection along the τ^+ direction (longitudinal polarization, $\mathbf{s} \cdot \hat{\mathbf{p}}$), $\theta_{D_s\tau}$ is the angle between the D_s^+ meson and the τ^+ lepton in the laboratory frame, and $\theta_{y,D_s\tau}$ ($\theta_{x,D_s\tau}$) its projection along the laboratory y (x) axis. All angles are small, $\mathcal{O}(10^{-3})$, due to the highly boosted D_s^+ mesons produced by the multi-TeV protons and the low Q -value of the D_s^+ decay. Rotational invariance in the τ^+ production and the fact that $\theta_{x,D_s\tau}$ is unconstrained in \mathbf{yz} planar channeling implies that s_x averages to zero, whereas s_z and s_y depend on momenta and $\theta_{y,D_s\tau}$, respectively, as shown in Fig. 2.

Very large samples of fixed-target $D_s^+ \rightarrow \tau^+ \nu_\tau$ events have been generated using PYTHIA [30], EVTGEN [31], and a fast simulation that generates phase-space kinematics. The τ^+ channeling has been simulated using the parameterization from Ref. [23], following the procedure described in detail in Ref. [13]. Here, a $L = 8$ cm long, $\theta_C = 16$ mrad bent Ge crystal tilted by $\theta_y = 0.1$ mrad, placed $L_{\text{tar}} = 8$ cm downstream of the $T = 1$ cm thick W target, has been taken. A signal polarized sample is obtained by selecting channeled τ^+ and imposing kinematic requirements on final state particles. For example, requiring the momentum of the 3π system to be higher than 1 TeV selects events with a \mathbf{z} polarization about 20% or higher. Instead, discriminating between positive and negative $\theta_{y,D_s\tau}$ angles, in the following referred to as θ_y tagging, brings a \mathbf{y} polarization about $\pm 40\%$ or higher.

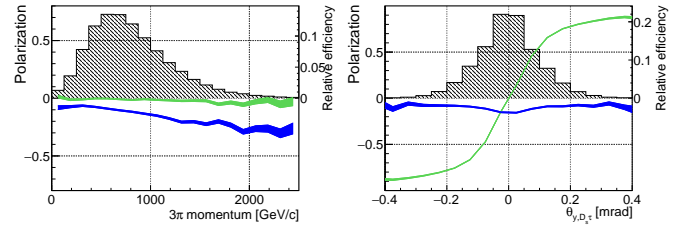


FIG. 2: Spin-polarization along the \mathbf{z} (blue regions) and \mathbf{y} (green) axes as a function of the momentum of the 3π system (left) and the $\theta_{y,D_s\tau}$ angle (right). The colored bands represent one-standard deviation regions arising from the limited simulation statistics. The hatched histograms show the spectra of the signal (channeled) τ^+ leptons, normalized to unity. The polarization along \mathbf{x} , not shown, is consistent with zero.

The spin-polarization precession induced by the interaction of the MDM and EDM of a relativistic, positively-charged particle channeled in a bent crystal was derived in [10] and proved to hold for non-harmonic potentials

in [13]. For the τ^+ lepton, the spin rotation for \mathbf{z} and \mathbf{y} initial polarization, $s_{0,z}$ and $s_{0,y}$ respectively, reads

$$\begin{aligned} s_x &\approx -s_{0,z} \frac{d'}{a_d} \sin \Phi + s_{0,y} \frac{d' a'}{a_d^2} (1 - \cos \Phi), \\ s_y &\approx s_{0,z} \frac{a'}{a_d} \sin \Phi + s_{0,y} \left(\frac{d'^2}{a_d^2} + \frac{a'^2}{a_d^2} \cos \Phi \right), \\ s_z &\approx s_{0,z} \cos \Phi - s_{0,y} \frac{a'}{a_d} \sin \Phi, \end{aligned} \quad (4)$$

where $a' = a + \frac{1}{1+\gamma}$, $d' = d/2$, $a'_d = \sqrt{a'^2 + d'^2}$, and $\Phi = \gamma\theta_C a'_d$ is the precession angle, with θ_C the crystal bending angle. These equations hold at $\mathcal{O}(10^{-2})$ level. Similar expressions retaining $\mathcal{O}(10^{-5})$ precision are reported in the supplemental material [32]. In the limit $(g-2) \gg 1/\gamma$, d and $s_{0,z} = 0$, Eq. (4) effectively reduces to that obtained in Refs. [10, 33].

The largely dominant contribution to the statistical uncertainty on a and d can be estimated from Eq. (4). For small Φ (as $\gamma\theta_C \sim 10$ and $a'_d \sim 10^{-3}$) and \mathbf{z} initial polarization,

$$\sigma_a \approx \frac{1}{S_y s_{0,z} \gamma \theta_C} \frac{1}{\sqrt{N_{\tau^+}^{\text{rec}}}}, \quad \sigma_d \approx \frac{2}{S_x s_{0,z} \gamma \theta_C} \frac{1}{\sqrt{N_{\tau^+}^{\text{rec}}}}, \quad (5)$$

where $N_{\tau^+}^{\text{rec}}$ is the number of channeled and reconstructed τ^+ leptons and S_i is the average event information [34] along a given crystal axis, discussed below. Analogously, for \mathbf{y} initial polarization,

$$\sigma_a \approx \frac{1}{S_z s_{0,y} \gamma \theta_C} \frac{1}{\sqrt{N_{\tau^+}^{\text{rec}}}}, \quad \sigma_d \approx \frac{2}{S_x s_{0,y} (\gamma \theta_C)^2 a'} \frac{1}{\sqrt{N_{\tau^+}^{\text{rec}}}}. \quad (6)$$

For given γ , $N_{\tau^+}^{\text{rec}}$, and initial polarization and average event information along the three axes, the sensitivities are similar except for d from \mathbf{y} polarization, which is disfavored by a factor ~ 10 .

An optimization of the crystal configuration has been performed for the case of initial polarization along \mathbf{z} . Using the simulation described earlier, the region of minimal uncertainty on a and d as given by Eq. (5) with $S_x = S_y$ is determined from a five-dimensional scan in the $(L, \theta_C, \theta_y, L_{\text{tar}}, p_{3\pi})$ parameter space. Here, $p_{3\pi}$ is the momentum of the visible hadronic system from the τ^+ decay. From the region of minimal error in the (L, θ_C) plane, shown in Fig. 3(left), we choose $\theta_C = 16$ mrad and $L = 8$ (11) cm for Ge (Si). Recently, first prototypes of Si and Ge crystals with similar parameters have been tested on beam at CERN H8 experimental area [35]. The scan for L_{tar} , shown in Fig. 3(right), reveals a wide plateau around the minimum placed close to 12 cm. Finally, minimal uncertainties are found for channeled events satisfying $p_{3\pi} > 800$ GeV/ c .

Table I reports the spin-polarization, channeling efficiency and average Lorentz boost, for Ge and Si crystals with optimal parameters, without and with θ_y -tagging.

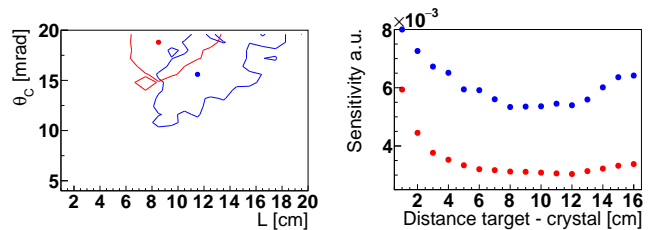


FIG. 3: Regions of minimal uncertainty for a and d as a function of the crystal parameters L and θ_C (left) and L_{tar} (right), for Ge (red) and Si (blue), for initial polarization along \mathbf{z} . The lines represent regions whose uncertainties on a and d are increased by 10% with respect to the minimum.

The Ge crystals provide enhanced channeling efficiency while keeping identical polarimeter characteristics, reaching -18% along \mathbf{z} . With θ_y -tagging, *e.g.* distinguishing positive and negative $\theta_{y,D_s\tau}$, a large \mathbf{y} polarization about $\mp 40\%$ can be additionally induced with an ideal tagging efficiency of 100%. Instead, a θ_y -tagging based on the requirement $\theta_{y,D_s\tau} \leq \pm 80$ μrad would enhance the \mathbf{y} polarization to $\mp 76\%$, decreasing the \mathbf{z} polarization to about -10% , with ideal tagging efficiency of 27%.

TABLE I: Average spin-polarization projections along \mathbf{z} and \mathbf{y} , channeling efficiency and average boost, for Ge and Si crystals with optimal parameters, without and with θ_y -tagging. Here, the θ_y -tagging labels events with $\theta_{y,D_s\tau} \leq \pm 80$ μrad . The \mathbf{x} polarization component is in all cases negligibly small.

	Ge	Ge θ_y -tagging	Si	Si θ_y -tagging
$s_{0,z}$	-0.175(9)	-0.096(11)	-0.175(15)	-0.114(20)
$s_{0,y}$	-0.013(6)	$\mp 0.759(4)$	-0.014(11)	$\mp 0.759(6)$
$\varepsilon_{\text{CH}} (\times 10^{-6})$	6.33(8)	1.67(4)	2.02(5)	0.56(2)
γ	812(3)	698(4)	800(5)	709(6)

Strategies for θ_y -tagging require information statistically correlated with the trajectory of the D_s^+ meson produced in the p -W hard interaction, projected along the yz plane. An option could be exploiting the tracks associated to the primary vertex where the D_s^+ is produced. Besides, the relatively large separation between the target and crystal, ≈ 12 cm, should allow to allocate additional apparatus, offering other options. For example, instrumenting with several layers of high granularity, extremely radiation-hard sensors, *e.g.* diamond detectors, would allow to provide information on the track left by the D_s^+ meson. Yet, another possibility would be to place a second bent crystal to channel the D_s^+ , along the lines suggested in [36]. Although this proposal, presented while completing the studies presented in this Letter, focuses on the τ^+ MDM, it could easily be adapted as a θ_y -tagger, at the cost of a low tagging efficiency. Indeed, with the optimal parameters reported ($L = 10$ cm, $\theta_C = 14.3$ mrad, $\theta_y = 180$ μrad for the main crystal, and

3 cm, 3 mrad, 100 μ rad, respectively, for the second) the channeling efficiency reduces to 2.8×10^{-7} for Ge, corresponding to a tagging efficiency of 3.6%.

The optimal polarization extraction technique for τ leptons [37] cannot be directly applied because the helicity angle of the 3π system is not precisely determined. A novel technique using multivariate classifier is explored to extract the τ^+ polarization without a-priori knowledge of the experimentally reconstructed $\tau^+ \rightarrow 3\pi\bar{\nu}_\tau$ decay distribution.

For each crystal axis, a classifier discriminating between τ^+ leptons fully polarized in the axis positive and negative direction is built. It is trained on simulated $\tau^+ \rightarrow 3\pi\bar{\nu}_\tau$ decays of channeled leptons passing the selection requirements. The classifier is based upon the variables describing the $\tau^+ \rightarrow 3\pi\bar{\nu}_\tau$ decay distribution, referred with the symbol ζ : two- and three-pion invariant masses, the angle between the 3π system and the crystal axis in the τ^+ rest frame, and the angles describing the 3π decay plane orientation in the 3π helicity frame reached from the τ^+ frame. The τ^+ rest frame is estimated applying a reconstruction algorithm that employs the 3π momentum, the τ^+ decay direction and the τ^+ mass constraint [38], in which one of the two solutions arising from the mass constraint is chosen randomly. In absence of the τ^+ production vertex, the decay direction is assumed to be that connecting the D_s^+ production vertex and the τ^+ decay vertex, lying in the crystal channeling plane. The vertex positions are smeared according to Gaussian distributions to mimic experimental resolutions, assumed to be 13 μ m and 70 μ m for production vertices in the longitudinal and transverse directions with respect to the beam, respectively, 100 μ m and 1 mm for decay vertices.

The polarization component s_i is extracted by fitting the classifier distribution $\mathcal{W}_i(\eta)$ on data, where $\eta \equiv \eta(\zeta)$ is the classifier response, with templates representing the response for ± 1 polarizations $\mathcal{W}_i^\pm(\eta)$,

$$\begin{aligned} \mathcal{W}_i(\eta) &= \frac{1+s_i}{2}\mathcal{W}_i^+(\eta) + \frac{1-s_i}{2}\mathcal{W}_i^-(\eta) \\ &= \frac{\mathcal{W}_i^+(\eta) + \mathcal{W}_i^-(\eta)}{2} + s_i \frac{\mathcal{W}_i^+(\eta) - \mathcal{W}_i^-(\eta)}{2}. \end{aligned} \quad (7)$$

The statistical separation between templates also represents the squared average event information or sensitivity to the polarization (at $s_i = 0$) from maximum-likelihood fits [37],

$$S_i^2 = \frac{1}{N_{\tau^+}^{\text{rec}} \sigma_i^2} = \left\langle \left(\frac{\mathcal{W}_i^+(\eta) - \mathcal{W}_i^-(\eta)}{\mathcal{W}_i^+(\eta) + \mathcal{W}_i^-(\eta)} \right)^2 \right\rangle, \quad (8)$$

where σ_i is the uncertainty on s_i .

The method is tested on simulated channeled lepton decays passing the selection requirements and compared against the analytical result. The \mathbf{x} and \mathbf{y} polarization components are correctly retrieved, *i.e.* consistent with

zero, while the \mathbf{z} component is overestimated by about a factor two. The template fits are shown in Fig. 4. Stud-

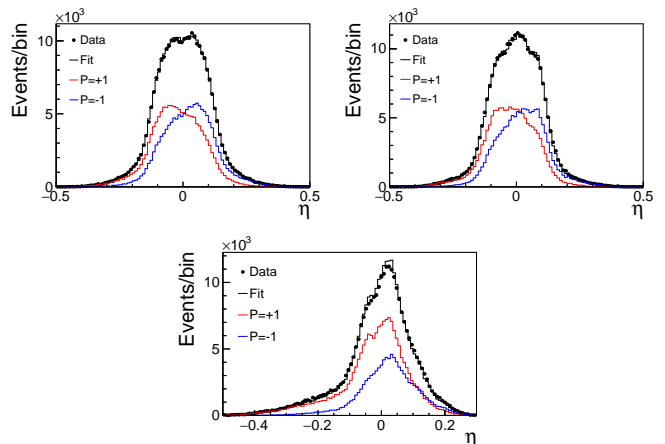


FIG. 4: Template fit to the classifier response on simulated events for \mathbf{x} (top left), \mathbf{y} (top right) and \mathbf{z} (bottom) components.

ies with variants of the reconstruction algorithm show that the hadronic helicity angle distribution with respect to the z axis is very sensitive to the estimation of the τ^+ rest frame, this leading to evident distortions between true and reconstructed distributions and in turn to a wrong polarization extraction; on the contrary, the helicity angles in the transverse directions are basically independent of the algorithm employed. The sensitivity S_i for the three classifiers is 0.23, to be compared to the optimal value 0.58 reached in case of perfect and complete reconstruction of the τ decay amplitudes [37]. The loss in precision due to both the imperfect reconstruction and the use of multivariate classifiers instead of the decay amplitude model is a factor 2.5. Further investigation is required to improve the average event information and reduce the overestimation of the \mathbf{z} polarization component.

The a and d sensitivities are assessed from a large number of pseudo-experiments generated and fit using a probability density function based on the spin precession equation of motion and an angular distribution proportional to $1 + S\mathbf{s} \cdot \mathbf{k}$, where \mathbf{k} represents the τ^+ direction in the D_s^+ helicity frame. This distribution is equivalent to the classifier strategy provided that the average information S for all components is known. Figure 5 illustrates the results as a function of the number of impinging protons for Ge with and without θ_y -tagging, for different values of the average event information; two tagging cases are shown: the first is based on a discrimination between positive and negative $\theta_{y,D_s\tau}$ and ideal efficiency of 100%, the second on the double crystal option proposed in Ref. [36] and outlined previously. A detector reconstruction efficiency of 40% is assumed. The corresponding sensitivities for Si are a factor 1.8 worse.

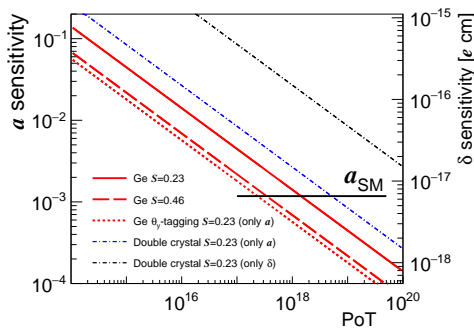


FIG. 5: Estimated sensitivities for a and d as a function of the number of protons on target (PoT) for a Ge crystal with optimal parameters, without and with θ_y -tagging, and different values of the average event information ($S = 0.23, 0.46$). The SM model prediction for a is also indicated.

The τ^+ leptons that are channeled are produced at very small angles with respect to the impinging proton beam, *e.g.* 100 μrad , and have large momentum, also above 1 TeV/c . The channeling process keeps the momentum unchanged while deflecting the particles at the bending angle $\theta_C \approx 16$ mrad. This signature can be identified in the $\tau^+ \rightarrow 3\pi\bar{\nu}_\tau$ decays through the reconstruction of the 3π momentum which, for highly boosted particles, also defines the τ^+ direction up to a difference of ≈ 0.51 mrad. The 3π common vertex identifies the decay position. By requiring simple kinematic cuts, the contribution of non-channeled particles is reduced to a negligibly small level $< 0.3\%$. The background has been suppressed using the following selection criteria: the 3π momentum greater than 800 GeV/c , its direction consistent with θ_C within 1.5 mrad, and the 3π vertex located after the crystal, at a distance $L + L_{\text{tar}} \gtrsim 20$ cm from the interaction point. Background contributions from channeled hadron decays, *e.g.* D^+ , D_s^+ mesons, Λ_c^+ baryons, are vetoed using the reconstructed invariant mass and the particle identification information. Another potential source of background comes from τ^+ leptons that are channeled only through a fraction of the crystal length. These are mainly events in which the D_s^+ decays inside the crystal or the τ^+ particle does not reach the end of the crystal channel, either because it decays or gets dechanneled. They compose 28% of the τ^+ candidate sample. Nevertheless, only τ^+ particles that travel almost through the entire crystal are selected with the applied cuts. They experience very similar electromagnetic field, inducing a relatively small bias on the spin precession angle Φ of 1.4% that can be corrected.

In summary, a novel method for the direct measurement of the τ^+ MDM and EDM has been presented with interesting perspective for a stringent test of the SM and search of new physics. The experimental setup and the analysis technique has been discussed along with sensitivity projections for possible future scenarios. The SM

prediction for the τ^+ MDM could be verified experimentally with a statistics around or exceeding 10^{19} PoT, whereas at the same time a search for the τ^+ EDM reaching 10^{-18} $e\text{ cm}$ level could be performed.

We express our gratitude for stimulating discussions to V. Baryshevsky, F.J. Botella, G. Cavoto, A. S. Fomin, A. Mazzolari and A. Pich. We acknowledge support from INFN (Italy), MINECO and GVA (Spain), the Severo Ochoa excellence certification SEV-2014-0398-01, and the ERC Consolidator Grant SELDOM G.A. 771642.

-
- [1] P. J. Mohr, D. B. Newell, and B. N. Taylor, *Rev. Mod. Phys.* **88**, 035009 (2016), 1507.07956.
 - [2] V. Andreev et al. (ACME), *Nature* **562**, 355 (2018).
 - [3] G. W. Bennett et al. (Muon (g-2)), *Phys. Rev.* **D73**, 072003 (2006), hep-ex/0602035.
 - [4] G. W. Bennett et al. (Muon (g-2)), *Phys. Rev.* **D80**, 052008 (2009), 0811.1207.
 - [5] J. M. Pendlebury et al., *Phys. Rev.* **D92**, 092003 (2015), 1509.04411.
 - [6] G. Schneider et al., *Science* **24** **358**, 1081 (2017).
 - [7] B. Sahoo, *Phys. Rev.* **D95**, 013002 (2017), 1612.09371.
 - [8] B. Graner, Y. Chen, E. G. Lindahl, and B. R. Heckel, *Phys. Rev. Lett.* **116**, 161601 (2016), [Erratum: *Phys. Rev. Lett.* **119**, 119901 (2017)], 1601.04339.
 - [9] V. G. Baryshevsky, *Phys. Lett.* **B757**, 426 (2016).
 - [10] F. J. Botella, L. M. Garcia Martin, D. Marangotto, F. M. Vidal, A. Merli, N. Neri, A. Oyanguren, and J. R. Vidal, *Eur. Phys. J.* **C77**, 181 (2017), 1612.06769.
 - [11] V. G. Baryshevsky, *Nucl. Instrum. Meth.* **B402**, 5 (2017).
 - [12] A. S. Fomin et al., *JHEP* **08**, 120 (2017), 1705.03382.
 - [13] E. Bagli et al., *Eur. Phys. J.* **C77**, 828 (2017), 1708.08483.
 - [14] V. G. Baryshevsky (2018), 1803.05770.
 - [15] M. A. Samuel, G.-w. Li, and R. Mendel, *Phys. Rev. Lett.* **67**, 668 (1991), [Erratum: *Phys. Rev. Lett.* **69**, 995 (1992)].
 - [16] E. Leader, *Spin in particle physics*, vol. 15 (Camb. Monogr. Part. Phys. Nucl. Phys. Cosmol., 2011), ISBN 9780511874185.
 - [17] A. Pich, *Prog. Part. Nucl. Phys.* **75**, 41 (2014), 1310.7922.
 - [18] S. Eidelman and M. Passera, *Mod. Phys. Lett.* **A22**, 159 (2007), hep-ph/0701260.
 - [19] W. Dekens, J. De Vries, M. Jung, and K. K. Vos (2018), 1809.09114.
 - [20] M. Tanabashi et al. (Particle Data Group), *Phys. Rev.* **D98**, 030001 (2018).
 - [21] J. Abdallah et al. (DELPHI), *Eur. Phys. J.* **C35**, 159 (2004), hep-ex/0406010.
 - [22] K. Inami et al. (Belle), *Phys. Lett.* **B551**, 16 (2003), hep-ex/0210066.
 - [23] V. M. Biryukov et al., *Crystal Channeling and Its Application at High-Energy Accelerators* (Springer-Verlag Berlin Heidelberg, 1997).
 - [24] R. Aaij et al. (LHCb collaboration), *Phys. Rev. Lett.* (2018).
 - [25] M. Lisovyi, A. Verbytskyi, and O. Zenaiev, *Eur. Phys. J.* **C76**, 397 (2016), 1509.01061.

- [26] L. Gladilin, Eur. Phys. J. **C75**, 19 (2015), 1404.3888.
- [27] C. Patrignani, Chin. Phys. **C40**, 100001 (2016).
- [28] F. Halzen and A. D. Martin, *Quarks and leptons: An introductory course in modern particle physics* (1984), ISBN 0471887412, 9780471887416.
- [29] V. B. Berestetskii, E. M. Lifshitz, and L. P. Pitaevskii, *Quantum Electrodynamics*, vol. 4 of *Course of Theoretical Physics* (Butterworth-Heinemann, Oxford, 1982), ISBN 0750633719.
- [30] T. Sjostrand, S. Mrenna, and P. Z. Skands, JHEP **05**, 026 (2006), hep-ph/0603175.
- [31] D. J. Lange, Nucl. Instrum. Meth. **A462**, 152 (2001).
- [32] See supplementary material for details.
- [33] There is a missing global minus sign in the s_x component in [10, 13].
- [34] M. Kendall, A. Stuart, and J. Ord, *The advanced theory of statistics* (1983).
- [35] A. Mazzolari et al., Private communication. Paper in preparation (2018).
- [36] A. S. Fomin, A. Y. Korchin, A. Stocchi, S. Barsuk, and P. Robbe (2018), 1810.06699.
- [37] M. Davier, L. Duflot, F. Le Diberder, and A. Rouge, Phys. Lett. **B306**, 411 (1993).
- [38] S. Dambach, U. Langenegger, and A. Starodumov, Nucl. Instrum. Meth. **A569**, 824 (2006), hep-ph/0607294.
- [39] L. H. Thomas, Nature **117**, 514 (1926).
- [40] L. H. Thomas, Phil. Mag. **3**, 1 (1927).
- [41] V. Bargmann, L. Michel, and V. L. Telegdi, Phys. Rev. Lett. **2**, 435 (1959).

Novel method for the direct measurement of the τ lepton dipole moments

The following includes supplementary material.

The time evolution of the spin-polarization vector \mathbf{s} is regulated by the T-BMT equation [39–41]. The precession of the spin-polarization vector induced by the interaction of the MDM and the EDM of a charged particle channeled in a bent crystal was derived in Ref. [10], assuming initial polarization along the \mathbf{y} axis and $(g-2) \gg 1/\gamma$, d . For the τ lepton, however, $a = (g-2)/2 \approx 10^{-3} \sim 1/\gamma$ and there is, in general, polarization along the \mathbf{z} and \mathbf{y} axes.

$$\begin{aligned}
 \frac{s_x}{s_{0,z}} &\approx \frac{d'}{a'_d} \left[-c \sin \Phi + \frac{a'}{a'_d} s (1 - \cos \Phi) \right] \approx -\frac{d'}{a'_d} \sin \Phi, \\
 \frac{s_y}{s_{0,z}} &\approx \frac{a'}{a'_d} \left[\sin \Phi + \frac{d'^2}{a'_d a'} s c (1 - \cos \Phi) \right] \approx \frac{a'}{a'_d} \sin \Phi, \\
 \frac{s_z}{s_{0,z}} &\approx \frac{a'^2}{a_d'^2} \left[\left(1 + \frac{d'^2}{a'^2} c^2 \right) \cos \Phi + \frac{d'^2}{a'^2} s^2 \right] \approx \cos \Phi,
 \end{aligned} \tag{9}$$

where $a' = a + \frac{1}{1+\gamma}$, $d' = d/2$, $a'_d = \sqrt{a'^2 + d'^2}$, and $\Phi = \gamma \theta_C a'_d$ is the precession angle, with θ_C the crystal bending angle. The coefficients s and c are given by $\sin(\overline{\Omega}t)$ and $\cos(\overline{\Omega}t)$, respectively, where $\overline{\Omega}t \approx c/\rho_0 \times L/c = \theta_C \sim 10^{-2}$, with ρ_0 (L) the crystal curvature radius (length), is the average rotation angle of the particle trajectory when traversing the bent crystal with revolution frequency Ω in a time interval t . For each component, the first expression holds at precision $\mathcal{O}(10^{-5})$, whereas the second approximation applies at $\mathcal{O}(10^{-2})$. Similarly, the spin motion for initial polarization along the \mathbf{y} axis, $s_{0,y}$, is given by

$$\begin{aligned}
 \frac{s_x}{s_{0,y}} &\approx \frac{d'}{a'_d} \left[\frac{a'}{a'_d} c (1 - \cos \Phi) + s \sin \Phi \right] \approx \frac{d' a'}{a_d'^2} (1 - \cos \Phi), \\
 \frac{s_y}{s_{0,y}} &\approx \frac{a'^2}{a_d'^2} \left[\frac{d'^2}{a'^2} c^2 + \left(1 + \frac{d'^2}{a'^2} s^2 \right) \cos \Phi \right] \approx \frac{d'^2}{a_d'^2} + \frac{a'^2}{a_d'^2} \cos \Phi, \\
 \frac{s_z}{s_{0,y}} &\approx \frac{a'}{a'_d} \left[-\sin \Phi + \frac{d'^2}{a'_d a'} s c (1 - \cos \Phi) \right] \approx -\frac{a'}{a'_d} \sin \Phi.
 \end{aligned} \tag{10}$$

In the limit $(g-2) \gg 1/\gamma, d$, Eq. (10) effectively reduces to that obtained in Refs. [10, 33].